PAPER

Check for updates

Microthermal catalytic aerogenesis of renewable biomass waste using cathode materials from spent lithium-ion batteries towards reversed regulated conversion and recycling of valuable metals†

Xiangping Chen, [ID] [a] Yi Wang,[a] Lu Yuan,[b] Shubin Wang, [ID] *[c] Shuxuan Yan,[d] Hongbo Liu[d] and Junhua Xu*[e]

Sustainable recycling of metal resources from spent lithium-ion batteries (LIBs) with reduced environmental impacts is attracting increasing attention in the current recycling processes. However, over-reliance on energy and chemical input is one of the leading bottlenecks for the prevailing technologies. In this study, pyrolysis gases generated from renewable biomass waste by microthermal catalysis of the cathode material ($LiNi_xCo_yMn_{1-x-y}O_2$) in spent LIBs were innovatively used as reactants for the regulated reduction and conversion of different metals. Detailed experimental results suggest that different reaction pathways for metals can be controlled by the experimental conditions, especially reaction temperature. Li tends to be converted into Li_2CO_3, immune to the reaction temperature, while Co(III) and Mn(IV) can be just reduced into CoO and MnO in the lower roasting temperature range of 300 °C–500 °C, with further reduction into their metallic forms Co and Ni in the higher temperature range of 500 °C–700 °C, while MnO cannot be further reduced into metallic Mn, and the different converted products are recovered based on their forms with significantly reduced consumption of chemicals. Finally, tentative exploration of the reaction mechanism suggests that cathode materials are efficient catalysts to reduce the roasting temperature and promote the generation of H_2 from biomass wastes, changing the traditional solid–solid reaction of carbothermal metallurgy to the gas–solid reaction of hydrogen metallurgy with reduced input of chemical and energy.

1. Introduction

As one of the most promising cathode materials applied in lithium-ion batteries (LIBs) with high energy density, $LiNi_xCo_yMn_{1-x-y}O_2$ (NCM) is widely assembled in hybrid electric/electric vehicles (HEVs/EVs) with its increasing share in

[a]*School of Environmental Science and Engineering, Shaanxi University of Science & Technology, Xi'an, Shaanxi Province, 710021, P.R. China*
[b]*College of Chemistry and Chemical Engineering, Hunan Normal University, Changsha, Hunan Province, 410081, P.R. China*
[c]*State Environmental Protection Key Laboratory of Environmental Pollution Health Risk Assessment, South China Institute of Environmental Sciences, Ministry of Ecology and Environment (MEE), Guangzhou, Guangdong Province, 510655, P.R. China. E-mail: wang.s.bean@gmail.com*
[d]*Hunan Provincial Key Laboratory of Chemical Power Sources, College of Chemistry and Chemical Engineering, Central South University, Changsha, Hunan Province, 410083, P.R. China*
[e]*Nuclear Chemistry & Separation and Purification Technology Laboratory, Fujian Institute of Research on the Structure of Matter, Chinese Academy of Sciences, Fuzhou, Fujian Province, 350002, P.R. China. E-mail: junhua.xu@fjirsm.ac.cn*
†Electronic supplementary information (ESI) available. See DOI: https://doi.org/10.1039/d2gc03947h

the global production and application.[1] Although these batteries exhibit excellent electrochemical performances, *e.g.* high energy capacity and voltage, favorable discharge resistance, high tolerance to a wide temperature range, and the fact that they are less harmful to the environment than other batteries,[2,3] a large quantity of spent LIBs has been inevitably discarded into the waste stream after the end of their life cycle for several years[4] and poses a severe risk towards the ecosystem and human beings because of their high levels of heavy metals and hazardous organics.[4,5] On the other hand, the availability of strategic metal resources (*e.g.* Li, Co, Ni) supplied for LIB manufacture is becoming a high priority for their global security supply.[6] There is, therefore, necessity for efficient and sustainable recycling of spent LIBs to ensure resource and environmental security.[7]

Currently, increasing efforts have been devoted to recycling different metal resources from waste NCM of spent LIBs for sustainable development of the new energy industry.[8] Hydrometallurgical, biohydrometallurgical and pyrometallurgical processes have been sophisticatedly adopted to recover the valuable metals.[9] As one of the most widely used conven-

tional recycling processes, the hydrometallurgical method usually involves the conversion of the target metals into lixivium, with subsequent separation of different metals from leaching solution. During leaching, mineral acids (*i.e.* H_2SO_4,[10] HCl,[11] HNO_3 [12] and H_3PO_4 [13]) and organic acids (*e.g.* citric acid,[14] oxalic acid,[15] and tartaric acid[16]) were sophisticatedly adopted as leachates, along with the addition of a reductant (*e.g.* H_2O_2[17] and glucose[18]) for the reductive leaching of NCM,[13] and different separation technologies, including precipitation,[19] solvent extraction[20] and electro-deposition,[21] were used for the recycling of valuable metals from leaching solution.[22,23] Although different metals can be recovered by the hydrometallurgical process with decent efficiency and selectivity, the extensive consumption of chemicals and tedious recycling procedures may result in secondary contamination, enhanced cost and loss of valuable metals.[24] Bioleaching is an emerging technology that is regarded as a promising alternative to leaching metals using microorganisms as acid producers,[25] while the slow kinetics, poor selectivity and high environmental sensitivity result in declined leaching efficiency, which also restricts its scaled-up application.[26] The pyro-metallurgical process usually involves high temperature treatments to refine or purify target metals.[27] Though thermochemical routes have high processing capacity and efficiency, extensive emission (*e.g.* SO_x) and volatilization of Li are inevitable in a high-temperature environment.[28–30] Therefore, the above issues concerning the extensive consumption of chemicals and energy, extended procedures, and unregulated selectivity and efficiency should be fully addressed for sustainably recycling valuable metals.

Increasing attention has been attracted by thermochemical reduction processes through microwave heating, vacuum pyrolysis and roasting by solid-to-solid reactions including carbothermal reduction,[8,31] thermite reduction,[4] sulfating roasting conversion[32,33] and biomass waste reduction[34,35] prior to hydrometallurgical extraction of valuable metals at high processing temperatures. On the other hand, the addition of reducing agents, *e.g.* Al foils (thermite reaction) and graphite (carbothermic reaction), increases the cost of the reaction and makes the subsequent separation process more difficult. For instance, a vacuum pyrolysis approach was adopted by Tang *et al.* to recover Li and Co from spent LIBs by mixing the as-received cathode materials (LiCoO₂, LCO) with graphite obtained from waste anode materials for selectively converting LCO into Co or CoO and Li_2CO_3 by carbothermic reduction from 873 K to 1273 K, with recovery rates of 93% and 99% for Li and Co.[31] Waste LCO was converted into $LiAlO_2$ and CoO at 600 °C for 60 min using Al foils as an *in situ* reductant, with leaching efficiencies of 94% and 96% for Li and Al achieved using 2.5 mol L⁻¹ NaOH as a leachant.[29] Zhang *et al.* reported chemical evolution of the $LiNi_{1/3}Co_{1/3}Mn_{1/3}O_2$–$NaHSO_4·H_2O$ system with a stoichiometric mass ratio of 1 : 4.3 in the reaction temperature range from 20 °C to 600 °C.[36] Although the above recycling technologies are available for the treatment of waste LCO, the increase of the valence of transition metals (Ni, Co and Mn) during the high-temperature preparation may lead

to the regeneration of strong Me–O chemical bonds and even adverse impacts on the subsequent leaching.[37,38] As typical renewable resources, biomass waste (BMW) was used as a promising additive during the thermochemical reduction process with the advantages of low cost, easy availability and eco-friendliness.[39,40] Besides, the adoption of BMW will also change traditional solid–solid reactions of carbothermal/thermite metallurgy into a mixed model of gas–solid/solid–solid reactions with reduced input of chemicals and energy. For example, BMW was used as the reductant during the reduction roasting of low-grade manganese dioxide ores at 500 °C for 80 min,[35] or as an alternative reductant for copper slag reduction (>1100 K).[34] However, the adoption of BMW as a reductant during thermochemical reduction processing of waste NCM from spent LIBs has rarely been reported. Pyrolysis and gasification of BMW to produce bioenergy, bio-oil, syngas, and biochar are among the most promising processes in thermochemical processes.[41,42] It is, therefore, necessary to explore possibilities for efficient conversion and reduction of different metals (Li, Ni, Co and Mn) in NCM using BMW as an effective and eco-friendly alternative, instead of the traditional chemical reductants.

In the present work, the thermochemical reduction process was proposed for the recycling of different metals from waste NCM using BMW (cornstalk) as the reductant. Different characterization methods namely TG-DSC, XRD and XPS were used to explore the detailed conversion and reduction process and the corresponding mechanism for different metals in NCM. Gas chromatography was applied to confirm gaseous products and explore the gas–solid reaction process. Thermodynamic data of the main reduction reactions during roasting were calculated using the HSC chemistry software. Different parameters namely reaction temperature, retention time and mass ratio of NCM : BMW on conversion and reduction of different metals, and acid concentration, pulp density, roasting temperature and mass ratio on the leaching of them were investigated to transfer Ni, Co and Mn with reduced valances in roasting products, after the water leaching of Li_2CO_3. Li and transition metals can be finally recovered as Li_2CO_3 and ternary precursors $Me(OH)_2$ (Me = Ni, Co and Mn), with significantly reduced consumption of chemicals and energy. It is expected that this recycling route involved low-temperature pyrometallurgical pretreatment and facile hydrometallurgical leaching can be a promising method for the selective conversion and recycling of different metals based on their natures with minimized chemical/energy consumption and environmental footprint.

2. Materials and methods

2.1. Materials and reagents

Waste NCM cathode materials (98 wt%) obtained after pretreatment through discharging, dismantling, peeling off Al foil, roasting and grinding were used as feed materials (Fig. S1†). The biomass waste corn stalk (CS, 20 mesh) was pur-

chased from Lianyungang, China (The choice of biomass wastes was clarified in our previous study.[43]). The elemental contents of NCM, BMW and mixed powders were determined using an ICP-OES (Intrepid II, American Thermofisher Company) and an Organic Element Analyzer (Elemeraor, Germany). The elemental contents are 30.61% Ni, 12.54% Co, 17.32% Mn and 1.82% Li for NCM, and 43.16% C, 4.05% H, 43.18% O and 1.04% N for CS. Their detailed compositions are listed in Table S1.† All the chemicals used are of analytical purity and purchased from Sigma Aldrich Co. Ltd, and deionized water was used for leaching, preparation of aqueous solutions and washing.

2.2. Experimental procedure

2.2.1. Thermochemical experiment. Quantitative amounts of waste NCM (4.00 g) and BMW (based on the mass ratio of NCM : BMW) were mixed and stirred for 10 min in a mortar to ensure their sufficient and homogeneous mixing. They were transferred into a quartz vessel and dried in an oven at 105 °C for 2 h. The as-prepared dried samples were used as feeds during thermochemical experiments. All the thermochemical experiments were conducted in a tube furnace (OTF-1200X, HF-Kejing) under a high-purity N_2 atmosphere. For each batch, the feeds were placed in the middle of a horizontal quartz tube, with the ventilation of high-purity N_2 for 15 min. Then, the feed materials were roasted to a set temperature at a heating rate of 10 °C min^{-1} (Maximum value), with further roasting at the set temperature for a controlled retention time. Different parameters, including roasting temperature, retention time and mass ratio, were investigated to achieve an all-around understanding of their effects on the conversion or reduction of different valuable metals. Solid samples obtained after the thermochemical experiments were used for the subsequent characterization and separation procedures, and the purified tail gases were collected using an airbag to determine

their composition. The self-designed equipment for the thermochemical experiment is shown in Fig. 1.

2.2.2. Selective recycling of different valuable metals. Firstly, the roasting products were intensively agitated in deionized water at room temperature for 3 h with a slurry density of 20 g L^{-1} to selectively extract Li_2CO_3 by water-leaching. Then, the products metallic Co and Ni were selectively separated by magnetic separation, and CoO, NiO and MnO in residues were dissolved using mild sulfuric acid. The product Li_2CO_3 in the aqueous phase can be directly obtained by evaporation, while transition metal enriched lixivium was used as the mother solution for the fabrication of ternary precursors.

The flowchart of the whole recycling route is illustrated in Fig. S2.† The conversion rate (Li_2CO_3) of Li (C) and purity of Li product (P) in the thermochemical process can be calculated using eqn (1) and (2), and the leaching rates (X_i) of transition metals (i = Co, Ni and Mn) can be calculated using eqn (3)

$$C_{Li} = \frac{m_{Li}\omega_{Li}}{m_0\omega_0} \times 100\% \tag{1}$$

$$P_{Li_2CO_3} = \frac{m_{Li}\omega_{Li}}{m_1\omega_1} \times 100\% \tag{2}$$

$$X_i = \frac{C_i V}{m_0\omega_i} \times 100\% \tag{3}$$

where m_0 and m_1 are the mass of feed materials and target product after thermochemical processing, g; ω_0 and ω_1 are the mass fraction of Li in feed materials and target product, wt%; m_{Li} is the mass of Li_2CO_3 obtained from water leaching, g; ω_{Li} is the mass fraction in Li_2CO_3, wt%; C_i is the concentration of the elements, g L^{-1}; V is the volume of lixivium, L; ω_i is the mass fraction of transition metals, wt%.
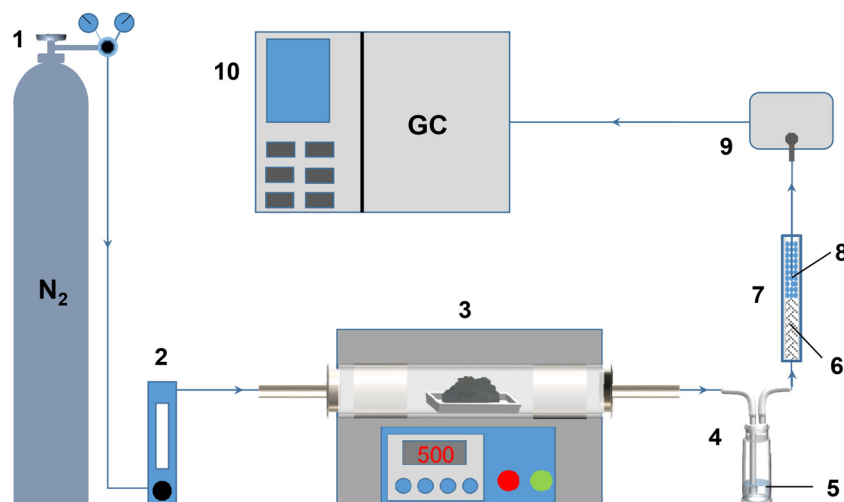

Fig. 1 The self-designed equipment for the thermochemical experiment (1. Nitrogen cylinder, 2. Gas flowmeter, 3. Glass tube furnace, 4. Gas-washing system, 5. Saturated sodium bicarbonate, 6. Skimmed cotton, 7. Drying tube, 8. Discolored silica gel, 9. Gas sample collection bag, 10. Gas chromatograph instrument).

2.3.　Analytical methods

In this study, different analytical methods were adopted to explore the thermochemical process and identify the obtained products. The contents of different metals in solid or aqueous samples were determined using an ICP-OES (Intrepid II, American Thermofisher Company). The HSC Chemistry 6.0 software was used to predict the Gibbs free energy of the related thermochemical reactions. A thermogravimetric analyzer (TGA/DSC3+, Switzerland) was applied to reveal the thermochemical characteristics and behaviors of feed materials with each batch heated from room temperature to 1000 °C at a heating rate of 10 °C min^{-1} under a N_2 atmosphere during the heating process. The gaseous products were analyzed by gas chromatography (GC, Agilent 7890B) using He as the carrier gas. Then, X-ray diffraction (XRD, D8 Advance, Bruker) and X-ray photoelectron spectroscopy (XPS, AXIS SUPRA) were employed for phase and valence state analyses of all feed materials and roasting products. The detailed information of the above instruments is given in Table S2.†

3.　Results and discussion

3.1.　Thermochemical experiments

In the roasting experiments, the effects of retention time, roasting temperature and mass ratio of NCM : BMW on the conversion of different metals were investigated to optimize the suitable experimental conditions (as shown in Fig. 2). It can be concluded from Fig. 2(a) that the addition of the BMW reductant can ensure the complete conversion of NCM into different products namely Li_2CO_3, MeO and Me (Me = Ni, Co or Mn), without an impurity phase formed during the reaction. The roasting products of Li_2CO_3, CoO, NiO and MnO can be simultaneously obtained at low mass ratios from 1 : 0.2 to 1 : 0.6, while metallic products Ni and Co is gradually formed with a gradual disappearance of Li_2CO_3 with the increase of the BMW dosage, indicating that the increased dosage of BMW restricts the generation of Li_2CO_3 and facilitates the deep reduction of transition metals, which may be caused by the screening effect of excessive BMW with the molecular structure of $C_xH_yO_z$.[40] The roasting temperature shows a significant influence on the formation of different products either (see Fig. 2(b)). With the increase of roasting temperatures in high levels (400 °C–700 °C), metallic Co and Ni tend to be formed along with the gradual shrinking of CoO and NiO, indicating that the higher roasting temperatures can facilitate the formation of metallic Co and Ni, but the diffraction peaks of MnO can be rather observed when the roasting temperature reaches over 650 °C. It is obvious that the reduction of Mn from the waste cathode material is much more difficult than the reduction of Ni and Co.[5] Simultaneously, the intensity of diffraction peaks for Li_2CO_3 also becomes stronger, which can be attributed to the possible shift of gas–solid reaction to solid–solid one of carbothermal reduction at a high temperature since BMW is eventually converted into biochar at high roasting temperatures and carbothermal reduction can effectively convert Co(III) and Ni(III) into metallic Co and Ni. However, the high roasting temperature will not only enhance energy consumption but also result in the loss of Li and secondary contaminations, which can aggravate the carbon footprint and decline the overall recovery efficiency.[44] Thus, lower roasting temperature and suitable BMW dosage should be adopted. As shown in Fig. 2(c), the moderate retention time of 15 min can ensure sufficient conversion of NCM into oxide and carbonate products while an extended reaction time results in the accumulation of metallic Co and Ni, which can be attributed to the change of traditional solid–solid reactions of carbothermal reduction into gas–solid reduction reactions by reducing gases through the gasification of BMW.

It can be discovered from the TG–DTG–DSC curves of spent NCM and mixed samples under the optimized experimental conditions that the weight losses of reductive roasting process mainly occurred in three stages (see Fig. 3(a)), namely the first stage 0–180 °C, the second stage 180–660 °C and the third stage 660–1000 °C. Actually, waste NCM is thermostable that can be hardly decomposed below 800 °C in inert gas due to its strong Me–O bond, and a little weight loss over 800 °C can be caused by volatilization of Li at such high temperatures.[45] The experimental results indicate that the addition of BMW can significantly reduce the decomposition temperature of NCM. Pyrolysis of BMW and decomposition of NCM can be regarded
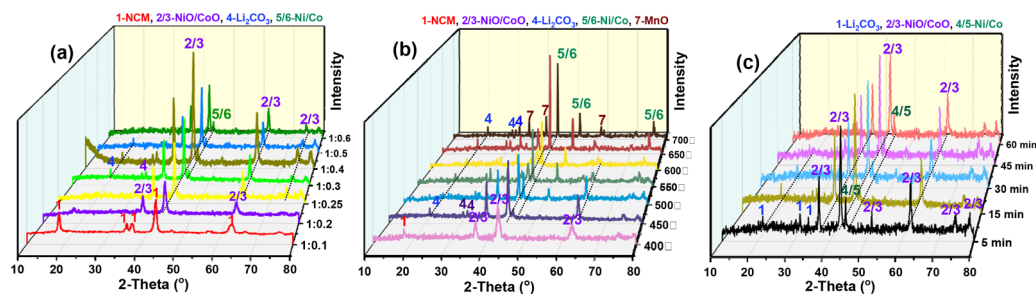

Fig. 2 The optimization of different parameters on the conversion of NCM into different products. (a) Effect of mass ratio of NCM : BMW (roasting temperature = 450 °C, retention time = 15 min); (b) effect of roasting reaction temperature (retention time = 15 min, NCM : BMW = 1 : 0.3) and (c) effect of retention time (NCM : BMW = 1 : 0.3, roasting temperature = 450 °C).
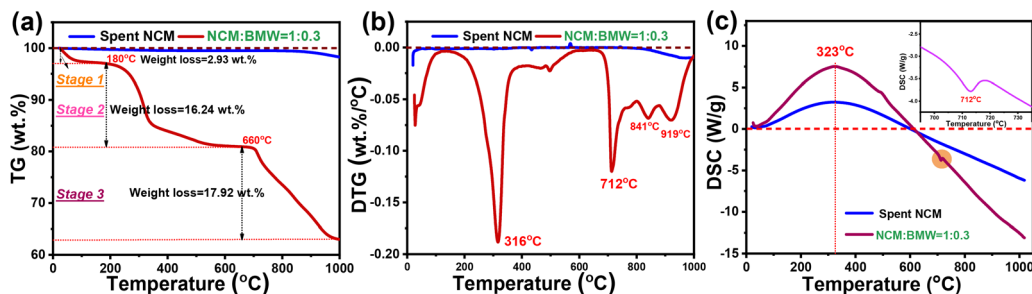
Fig. 3 The TG curve (a), DTG curve (b) and DSC curve (c) for cathode materials and roasting sample (heating rate – 10 °C min^{-1} and NCM : BMW = 1 : 0.3).

as the associated reactions,[46] which can significantly reduce the decomposition temperature of NCM from 1000 °C to 450 °C. In the first stage (0–180 °C), the weight loss is attributed to the removal of free/bonding water from BMW with dehydration and glass transition processes, which is a rapid process for the reduction of polymerization degree.[47] Only minor weight loss (<3 wt%) and small amounts of carboxyl groups, peroxy hydroxy groups and H_2 are generated in this stage.[44] The second stage is the pyrolysis process of BMW with the generation of large amounts of the cracked gases (*e.g.* H_2, CO, CO_2, CH_4) and the reducing gases immediately participate in reductive roasting reactions with the conversion of NCM into different roasting products. Weight loss in this stage becomes much more evident due to the volatilization of cracked gases. Actually, weight of the roasting products in this stage becomes heavier than that of NCM itself due to carbon fixation of Li and formation of L_2CO_3. It can be concluded from Fig. 3(b) that roasting temperatures at the maximum weight loss ratio are similar (around 316 °C), which can further prove that the dominant reaction in this stage is the pyrolysis of BMW. In this stage, it can also be found from Fig. 3(c) that the strongest exothermic peaks emerge at around 323 °C, which also coincides with the roasting temperature with the maximum weight loss ratio. Compared with the solid reductants (*e.g.* C, Al), the gaseous reductants (*e.g.* H_2 and CO) demonstrate a stronger reducing capacity even at low temperatures, promoting the decomposition of cathode materials and reducing the energy consumption of NCM during thermochemical process.[44] After the pyrolysis of BMW in Stage II, most volatile substances in BMW are converted into gases, leaving the non-volatile substances (biochar) as the roasting products. Then, biochar (C) can further react with the roasting products CoO, MnO_2 and NiO in Stage III. In this stage, CoO and NiO are reduced into Co and Ni, resulting in a significant weight loss of 17.92% with the conversion of oxides into metals. Besides, these roasting reactions changed from endothermic to exothermic nature with the increase in temperature, indicating that the energy consumption of the roasting process in Stage III becomes self-sufficient.

Finally, GC was applied to determine the contents and composition of pyrolysis gases. The mixed sample (NCM : BMW = 1 : 0.3) and the biomass sample (blank) are compared with

respect to the yield of different gases (CO_2, CO, CH_4 and H_2) in the range of 400–700 °C (see Fig. 4). From Fig. 4(a) and (b) the yield of CO_2 and CO starts to increase sharply at 600 °C for the mixed sample, which is due to the carbothermic reduction reaction that promotes the production of CO and CO_2. From Fig. 4(c) and (d), it can be discovered that the gaseous composition of CH_4 and H_2 shows sudden upward trend in the temperature range of 450–500 °C, which is much higher than that for the blank group. Then, it drops sharply at 500–700 °C. This phenomenon is attributed to the characteristics of catalytic pyrolysis and gasification of transition metal oxides in NCM, and the catalytic pyrolysis reaction can increase both the carbon conversion and reaction rate for the Ni-based catalyst,
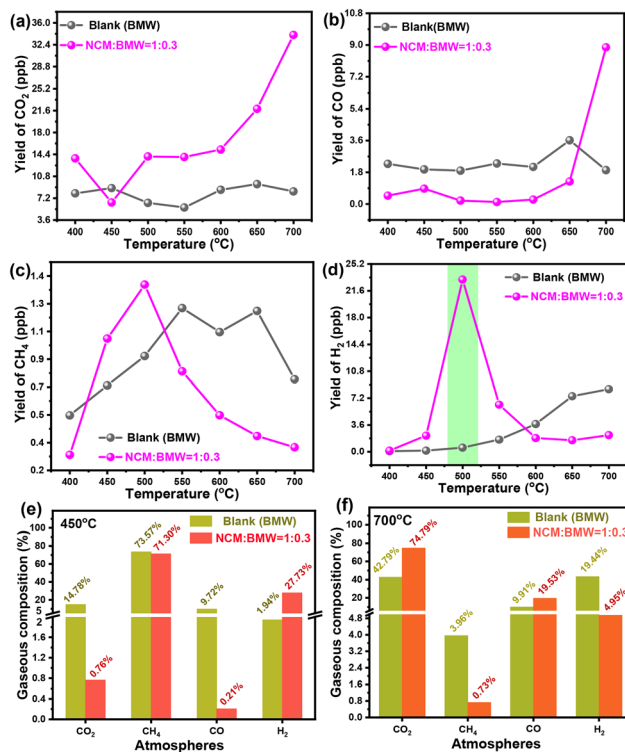

Fig. 4 Analytical results of GC: the yield of different gases from the blank sample and the mixed sample at different temperatures ((a) CO_2; (b) CO; (c) CH_4; (d) H_2; (e) 450 °C; (f) 700 °C).

which has remarkable advantage of high activities for tar cracking and methane reforming.[48] Fig. 4(e) shows the proportion of each gas in each group at a low roasting temperature (450 °C). The gas composition of CO_2, CH_4, CO and H_2 in the blank group is 14.78%, 73.57%, 9.72% and 1.94%, respectively. It is evident that almost all of CO and CO_2 are consumed after adding NCM at a roasting temperature of 450 °C, and CO is fully involved in the reduction reaction, while CO_2 is involved in the formation of L_2CO_3. The content of CH_4 shows a very small change, indicating that it is an inert gas at low temperature. However, the content of H_2 increases from 1.94% to 27.73% in the presence of NCM. NCM or transition-metal oxides have a certain catalytic effect to promote the production of small-molecule compounds, like H_2, through dehydration, decarboxylation, oligomerization and deoxygenation.[41] Thus, it is necessary to further investigate the catalytic effect of NCM that is more effective for cracking large-molecular gases into small-molecular ones. At a high temperature of 700 °C (see Fig. 4(f)), the yield of CH_4 and H_2 decreases compared with that in the control group, while the yield of CO and CO_2 shows an opposite increasing trend. This can be attributed to the carbothermic reduction reaction at high temperatures which promotes the production of CO and CO_2.

3.2. Conversion and reduction of different metals

During the reductive roasting process, the valence states and existing forms of Ni, Co and Mn in NCM are also changed along with the pyrolysis of BMW. The high-resolution XPS spectrum was used to explore changes in thermochemical

reaction under the experimental conditions of a roasting time of 15 min and an NCM : BMW mass ratio of 1 : 0.3 at different reaction temperatures (500 °C–700 °C) (see Fig. 5). As for the C 1s spectra shown in Fig. 5(a), the characteristic peak assigned to C at 284.8 eV corresponds to conductive carbon in NCM. The characteristic peak of C 1s1/2 at 289.8 eV corresponds to CO_3^{2-}.[49] Additionally, the high-resolution XPS spectra of C 1s confirm that a portion of C element is converted into carbonate (Li_2CO_3) after activation at 500–700 °C (Table S3†). Fig. 5(b) shows the Ni 2p spectra of NCM and its reduction products. The peaks at 856.8 eV in accordance with Ni 2p3/2 in NCM are assigned to Ni(III).[5] As shown in the spectra of the reduction products at 500 °C, the corresponding peaks of Ni(III) disappear and the Ni 2p spectrum has two main peaks located at 854.7 eV (2p3/2) and 872.3 eV (2p1/2) corresponding to NiO.[1] With the continuous increase in temperature, the characteristic peak of Ni (852.6 eV) appears at 600 °C, and the concentration of Ni increases at 650 °C (Table S4†). The Co 2p XPS spectra before and after roasting are illustrated in Fig. 5(c). The characteristic peaks at 780.1 eV and 795.24 eV in accordance with Co 2p3/2 and Co 2p1/2 in NCM are assigned to Co(III). As for the reduction product at 500 °C, the Co 2p3/2 binding energy at 778.3 eV is in accordance with zero-valent Co,[50] while the composition of CoO (796.6 eV) is still the dominant composition at 550 °C–600 °C. The peak fitting results indicate that the main peak for Co 2p3/2 can be split into peak 1 and 2, while the main peak for Co 2p1/2 can be split into peak 3 and 4 (see Table S5†), which is the same with the other elements. The spectrum of Mn 2p (see Fig. 5(d)) reveals the
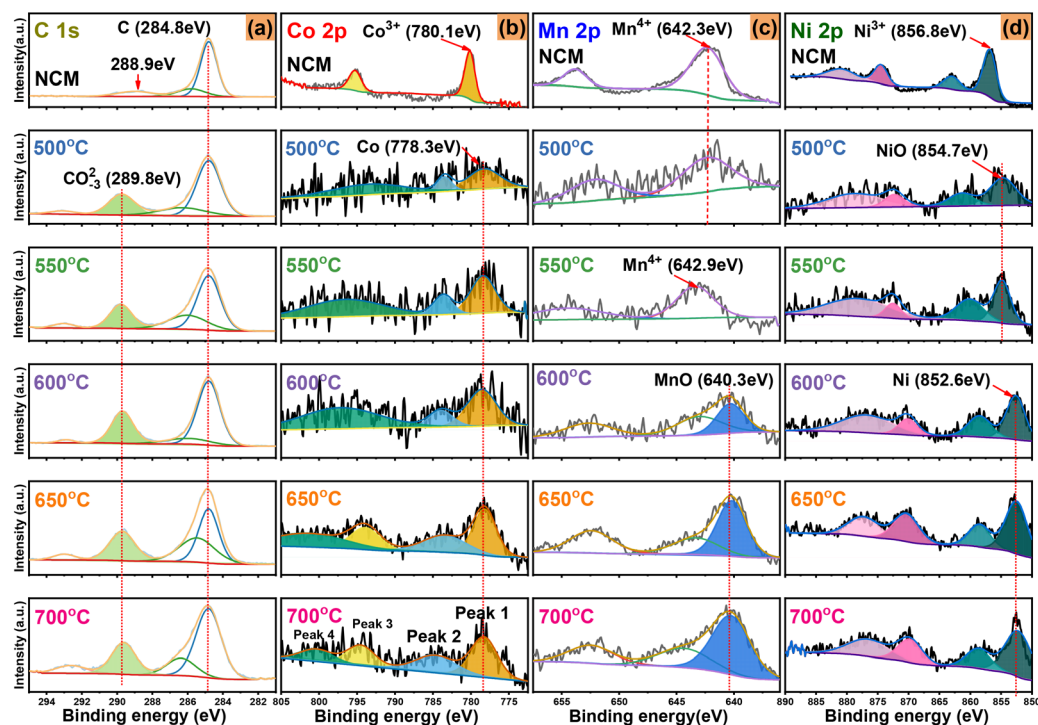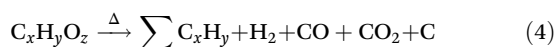

Fig. 5 High-resolution XPS spectra of (a) C 1s, (b) Co 2p, (c) Mn 2p and (d) Ni 2p of the NCM powders at different roasting temperatures.

peaks of Mn 2p3/2 and Mn 2p1/2 at 642.3 eV and 653.8 eV, assigning to manganese oxide.[4] After the reduction roasting at 600 °C, the Mn 2p3/2 binding energy appeared at 640.3 eV is the characteristic peak for MnO,[50] and its concentration gradually increases from 500 °C to 700 °C (Table S6†). Therefore, from the XPS spectra of Ni 2p, Co 2p and Mn 2p, it is obvious that low-valent transition metal oxides (NiO, CoO and MnO) and metal phases of Ni and Co co-exist in the reduced products with different contents; these results also agree with the analytical results of XRD.

Based on the above results, the thermodynamics of reactions was investigated based on the reduction roasting using BMW and NCM. Gibbs free energy was used to evaluate whether a certain chemical reaction proceeds spontaneously and to compare which reaction is the thermodynamically favorable one.[51] However, reactants are rarely in the corresponding standard states. As a rule of thumb, if standard Gibbs free energy ($\Delta_r G_T^\theta$) is less than -40 kJ mol^{-1}, Gibbs free energy ($\Delta_r G$) is usually less than 0. Based on this assumption, the standard Gibbs free energy can be used to determine whether a reaction is spontaneous.[52] The HSC Chemistry 6.0 was applied to analyze the relationship between the reaction temperature and the Gibbs free energy ($\Delta_r G$) for each reaction during roasting. When a chemical reaction reaches its equilibrium state, while $\Delta_r G < 0$, it indicates that the chemical reaction is spontaneous, and *vice versa*. The above analytical results show that reducing gases (*e.g.* H$_2$, CO) and biochar (C) are the dominant reducing substances that participate in reductive roasting reactions and chemical reaction during roasting, and the reductive roasting reaction can be described as follow:

$$C_xH_yO_z \xrightarrow{\Delta} \sum C_xH_y + H_2 + CO + CO_2 + C \quad (4)$$

The reduction roasting of NCM with BMW can be described as follows:

$$LiNi_xCo_yMn_zO_2 + H_2 + CO + CH_4 + C \xrightarrow{\Delta}$$
$$Li_2O + NiO + CoO + MnO + CO_2 + O_2 + H_2 \quad (5)$$
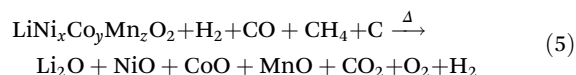
Possible chemical reactions and the corresponding changes of the Gibbs free energy of reaction under the standard conditions in the thermochemical process are listed in Table S7.†

Fig. S3† illustrates the detailed calculation results based on the above reactions. Gibbs free energies of Reaction (6)–(8) (**Hydrogen reduction process**, Table S7†) are negative at reaction temperature <380 °C, indicating that this reaction tends to proceed at lower reaction temperatures, which can significantly reduce the roasting temperatures than those in the reported thermite and carbothermal reduction reactions.[4,53] CO can easily participate in the reduction reaction, which can occur at very low temperatures (Fig. S3(b),† **Carbon monoxide reduction process**). As for related carbothermal reduction reactions – Reaction (13)–(18) (Table S7†), the initial reduction temperature is much higher (445 °C for Reaction (14) and 500 °C for Reaction (17)) than that for H$_2$ and CO reduction,

indicating that much higher roasting temperatures are required to start the reductive reactions. However, the relatively low reductive roasting temperatures for Reaction (13) and (18) (186 °C and 247 °C) can be ascribed to spontaneous reductive roasting process by CO reduction because C should firstly convert into CO and then participate in the further reduction process. In the case of high temperatures (465 °C and 630 °C), reduction reactions involving CH$_4$ can proceed spontaneously. Hydrogen reduction and carbon monoxide reduction can proceed at relatively low temperatures, while relatively high temperatures are required for the carbothermal and CH$_4$ reduction processes. Therefore, it can be concluded that all the above reduction reactions are competing reactions in the order of CO$_2$ > CO > H$_2$ > CH$_4$ > C, the Li is converted into Li$_2$CO$_3$ spontaneously and CO reacts with transition metals before H$_2$. CH$_4$ tends to be converted into H$_2$ through the catalytic effect of NCM and its derivants. All these reasons contribute to the accumulation of H$_2$, with the continuous production of hydrogen gas and non-spontaneous reactions with metals, giving H$_2$ as the final gas. Meanwhile, it can also be discovered from these equations that Li can only react with CO$_2$ to form Li$_2$CO$_3$ and it can be used as the adsorbent of CO$_2$. Ni and Co are in the same group, group VIII, indicating that they are similar in chemical properties. This leads to the conversion of Ni and Co in the same form (MeO or Me). However, Mn is different from Li, Ni and Co, and it can be seen that Mn remains in its high valence state Mn(IV); upon reduction, it should be firstly converted into Mn(II) and then into Mn, indicating that Mn cannot be easily reduced into its metallic form. This leads to its different form of existence from those of Co and Ni. Therefore, different metals are converted into different forms, and the conversion and recycling of Mn are different from those of Ni and Co. Different metals in waste NCM tend to be converted into different forms. The presence of Li in LCO is in the form of Li$_2$O, which will be gradually converted into Li$_2$CO$_3$, while transition metals are reduced according to Reaction (5).

The SEM images, EDS analysis and TEM images of various elements in waste NCM and roasted products under the optimized roasting conditions are presented in Fig. 6. It indicates that the mass fraction of Ni, Co and Mn in waste NCM is 13.7%, 18.52%, and 30.97%, respectively, without any impurity elements detected. The mass fraction of each metal in the roasted product at a temperature of 500 °C is reduced, with an increased weight ratio of O, indicating the formation of the metal oxides (NiO, CoO and MnO). The mass fractions of Ni, Co and Mn increase again in the roasting products at a temperature of 700 °C with a decreased weight ratio of O, indicating the reductive roasting process of NiO → Ni and CoO → Co. After the reduction roasting, the morphologies of NCM are significantly changed, with destroyed structure and new metal compounds formed as shown in the SEM images. Fig. S4† shows the EDS images of NCM and roasting products (500 °C and 700 °C). They indicate that the distribution of Ni, Co, Mn, O and C elements and the analytical results of EDS show that the mass fractions of Ni, Co and Mn decline significantly.
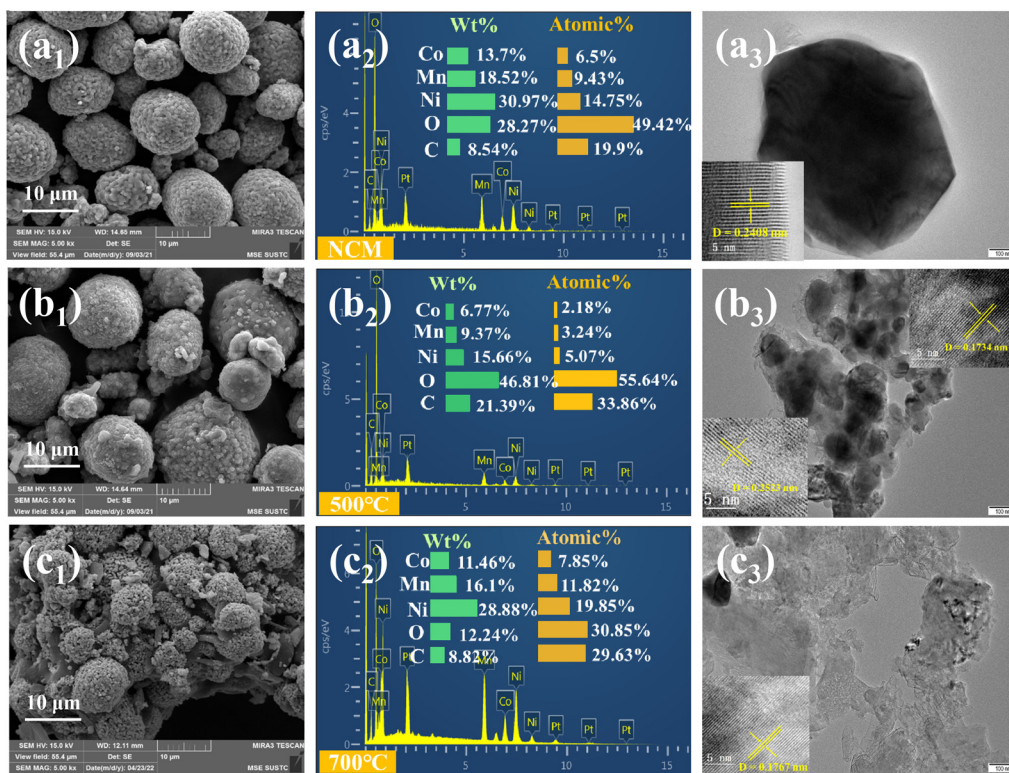
Fig. 6 SEM image, TEM image and corresponding EDS analysis of various elements in (a). Spent cathode material; (b). Roasted product at 500 °C, 15 min, NCM/BMW = 1 : 0.3; (c). Roasted product at 700 °C, 15 min, NCM/BMW = 1 : 0.3.

Besides, the contents of O and C increase significantly. The EDS (mapping) analysis of the specific atomic percentages of Ni, Co, Mn, O and C also suggests that waste NCM is converted into transition metal oxide components and the biochar produced from the pyrolysis of BMW leads to the increase of the carbon content. The HRTEM image (Fig. 6(a_3)) shows a lattice fringe spacing of 0.2408 nm, which is consistent with the Li ($Ni_{0.6}Co_{0.4})O_2$ (101) and $Li_4Mn_5O_{12}$ (311) planes. The fringe spacings of 0.2523 nm at 500 °C are consistent with the NiO (101) and CoO (111) planes, while the lattice fringe spacings of 0.1734 and 0.1767 nm are in line with the Ni (200) and Co (200) planes at 700 °C (Fig. 6(c_3)). This can further prove that the crystal structures in waste NCM are destroyed to generate metal oxides or metals.

3.3. Selective recycling of different metals

After reductive roasting, waste NCM was completely decomposed and transformed into NiO, CoO, MnO and Li_2CO_3 at moderate reaction temperatures of 300 °C–500 °C, or Ni, Co, MnO and Li_2CO_3 at elevated reaction temperatures of 500 °C–700 °C. Then, different recycling approaches were established, based on formations of these converted products after roasting processing. Water leaching was firstly applied to extract Li from all kinds of roasting products. It is clear that the conversion rate of Li increases with the increase of the roasting temperature from 450 °C to 550 °C and all Li is converted into Li_2CO_3 at 550 °C (see Fig. 7(f)) and a mass ratio of 1 : 0.3 in a

roasting time of 15 min, with a high purity of 99.99%. The effects of H_2SO_4 dosage, pulp density, roasting temperature and mass ratio on the leaching of transition metals were investigated. It can be found from Fig. 7(a)–(c) that a maximum leaching efficiency of 97.46%, 95.84% and 91.28% for Co, Ni and Mn, respectively, can be achieved at slurry densities of 30 g L^{-1} and 0.40 mol L^{-1} H_2SO_4. Besides, it can also be concluded that the leaching efficiency for Co and Mn is always lower than that for Ni at different roasting temperatures and mass ratios (see Fig. 7(d) and (e)), which can be caused by the different valence states of the transition metals, that is, Ni is in the lower valence state of Ni(II), while Co and Mn are in their high valence states (*i.e.* Co(III) and Mn(IV)). The pre-reduction of NCM can reduce the valence states of Co and Mn, which can indirectly improve the leaching efficiency. It can be concluded that Li was selectively extracted as Li_2CO_3 enriched lixivium after water leaching and transition metals were leached in a mildly acidic solution without the addition of reductants. Besides, the leaching kinetics of transition metals Ni, Co and Mn was investigated by correlating experimental data at various times (1 to 5 min) and temperatures (30–60 °C) for the diffusion model, and the fitting results show that the diffusion model fits the experimental data best with correlation coefficients over 0.95 (R^2) (see Fig. S5(a)–(c)†). The plot of ln *k vs.* 1000/*T* shows good fitting degrees ($R^2 > 0.91$) (see Fig. S5(d)–(f)†). The apparent activation energy (E_a) of Co, Ni and Mn is 39.64 kJ mol^{-1}, 42.12 kJ mol^{-1} and 42.03 kJ mol^{-1},
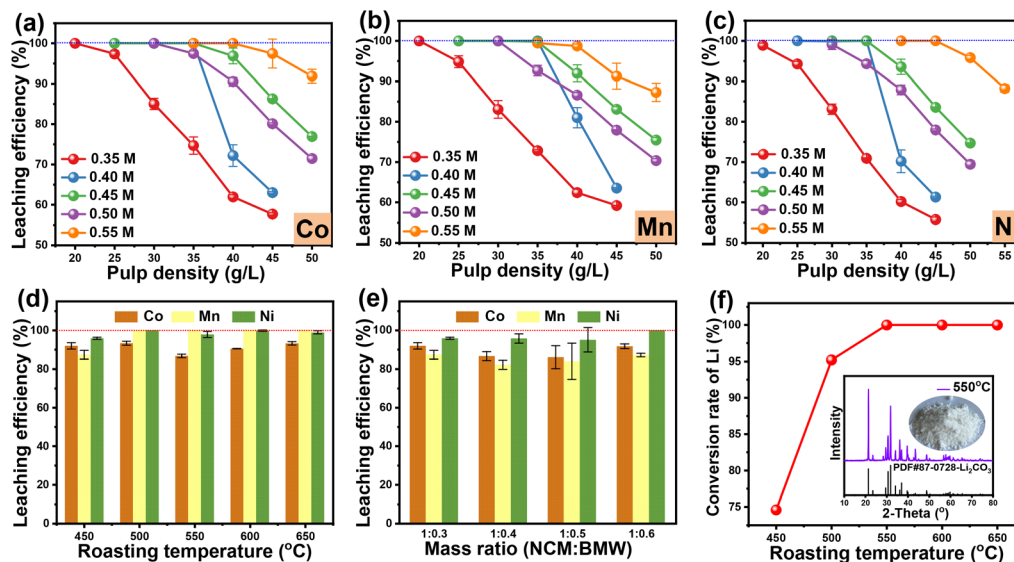
Fig. 7 Effects on the leaching efficiency of (a) Co, (b) Mn, (c) Ni (roasting temperature = 450 °C, NCM : BMW = 1 : 0.3, retention time = 15 min, leaching temperature = 50 °C, leaching time = 30 min), (d) (NCM : BMW = 1 : 0.3) and (e) (roasting temperature = 450 °C) and conversion rate of (f) Li at different roasting temperatures.

respectively. The relatively lower E_a values indicate that Ni, Co and Mn can be easily leached in this system.[54] Finally, the high value-added product Li_2CO_3 with high purity (99.99%) was recovered by evaporating the Li-enriched lixivium, and it can be re-used as battery-grade lithium carbonate for the re-fabrication of NCM (see Fig. S6(a)–(b)†), while the transition metal enriched could be directly recovered as $Ni_xCo_yMn_{1-x-y}(OH)_2$ precursors after adjusting the molar ratio of different transition metals, with reduced alkali consumption due to the reduced acid consumption during leaching. The products of Li_2CO_3 and $Ni_xCo_yMn_{1-x-y}(OH)_2$ could be directly reused as raw materials for the preparation of new NCM. In particular, metallic Ni/Co and MnO could be obtained (see Fig. S6(c)†) at a high roasting temperature of 700 °C, and the separation of transition metals could be followed by a first magnetic separation of Ni/Co and then mild acid leaching of MnO after water-leaching of Li. Therefore, Li_2CO_3, metallic Ni/Co and $MnSO_4$ were the specifically recovered products at a high roasting temperature of 700 °C.

3.4. Mechanism of microthermal catalytic aerogenesis and metal conversion

We then explored the detailed mechanism for the synchronized process of microthermal catalytic aerogenesis for BMW and metal conversion/reduction for NCM and its derivants; Fig. 8 summarizes the detailed mechanism and relationship between them to describe their synergetic effects on NCM and its derivants (*e.g.* NiO, CoO) for the improvement of H_2 composition and yield, and their thermochemical reduction and conversion with pyrolysis gases (*e.g.* CH_4, CO_2, CO, H_2). It can be concluded that the pyrolysis and gasification temperature of BMW (volatiles from the pyrolysis stage enters into the reforming stage) can be reduced due to the reduced activation ener-

gies in the existing forms of NCM and its derivants.[55,56] When the volatiles from BMW during the pyrolysis stage enter into the reforming stage, NCM ($LiNi_xCo_yMn_{1-x-y}O_2$), Ni/NiO and Co/CoO (as the active cores) can accelerate the reaction rates of different reactions through the reduction of activation energy,[57–59] which has been confirmed by the thermochemical experiment (reduced reaction time of 15 min and pyrolysis temperature of 450–500 °C). Here, the microthermal pyrolysis of BMW can be realized during the catalytic aerogenesis process activated by NCM and its derivants. BMW ($C_xH_yO_z$) is firstly cracked into C (biochar), C_nH_m (hydrocarbon), H_2O and other gases (*i.e.* CO, CO_2, CH_4 and H_2), and the composition and yield of the gaseous products are changed based on their properties during reforming reactions with the significantly increased proportion of H_2 at a pyrolysis temperature of 450 °C and CO_2 at a pyrolysis temperature of 700 °C, these results also match well with the experimental results shown in Fig. 4. Simultaneously, the cracked or reformed gases participate in the thermochemical reactions with NCM and its derivants during the entire reduction and conversion process. Specifically, it can be divided into two stages, namely the reduction and conversion of NCM into CoO, NiO, MnO and Li_2CO_3 in the low temperature range of 300 °C–500 °C by the gaseous products CO, CO_2, CH_4 and H_2. Only the oxides (MeO, Me = Ni, Co and Mn) and Li_2CO_3 are obtained in this stage, and generated CO_2 is directly adsorbed by Li_2O to form its carbonate that can be used as the roasting product. With the increase of the roasting temperature, CoO and NiO can be further reduced to metallic forms (Co and Ni), while MnO and Li_2CO_3 cannot be further converted into other forms, indicating that the separation of Mn from Ni and Co can be easily achieved by magnetic separation method from the roasting product at elevated reaction temperature. In summary, a dual
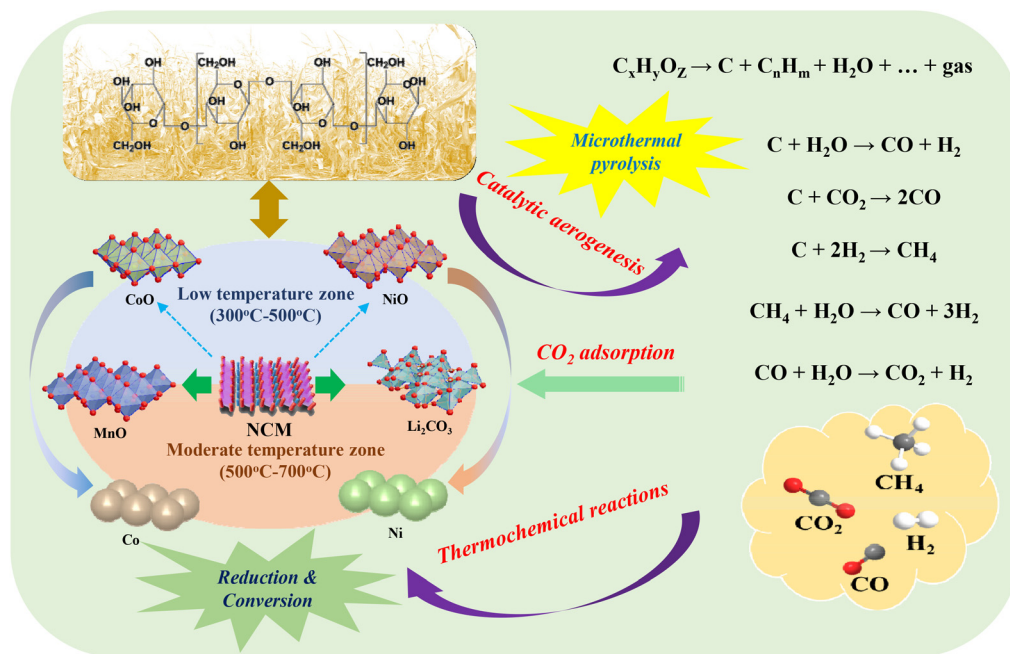
Fig. 8 Possible microthermal catalytic aerogenesis and metals conversion mechanism of BMW using waste NCM and its derivants as catalysts through thermochemical reactions.

interaction of BMW and NCM, with reduced pyrolysis temperature by the catalytic effect of NCM and its derivants, and a reverse reduction and conversion of different metals into the desired roasting products, can realize the maximized utilization and conversion of different kinds of wastes into valuable products (metal products from NCM and H_2 from BMW) with theoretical and experimental basis.

3.5. Economic assessments and environmental impacts

A brief economic assessment was conducted to evaluate the cost and revenue of the whole recycling process (Fig. S7†). Here, 1.0 kg of spent NCM batteries was used as the standard processing volume for calculation, and the main cost of this recycling process includes the chemical and raw material cost, energy consumption and environmental cost (see Tables S8 and S9†), with 3 main processes, namely thermochemical process, leaching & separation process and product refining process. In the first process, *i.e.*, thermochemical treatment, 0.50 kg of BMW and 1.00 kg is NCM are the input materials, and energy consumption is the dominant cost. The above-roasted products were used as raw materials for the subsequent separation of Li and transition metals, and the costs mainly include those for the consumption of chemicals and energy. Finally, the recovered products are Li_2CO_3, ternary precursors (at low roasting temperature) and Co/Ni/MnSO$_4$ (at high roasting temperature). The gross profit for each of the above processing routes in low or high roasting environments is $ 9.9 and $19.38, respectively (Table S10†). Table S11† shows that the recycling process was likely to involve waste solid, waste solution and waste gas; according to waste management, the disposal price of waste solid, waste solution and waste gas

is 147.1 $ per t, 0.411 $ per t and 92.88 $ per t, respectively. So, the input cost is about $ 0.02 for waste solid (0.15 kg), $ 0.01 for waste solution (20 L) and $ 0.99 for waste gas (10.69 kg). Besides, it can be concluded from a brief comparison of this study with previous ones (see Table S12†) that this work can significantly reduce the pyrolysis/roasting temperature and chemical consumption, with promoted reaction rates (less reaction time is required) and recyclable products that can be easily separated from each other. Besides, it can be also concluded from economic assessments and parallel comparison that this thermochemical recycling process reciprocally driven by low-temperature catalysis and conversion of BMW and NCM is a green, efficient and profitable method for recycling spent LIBs.

As for the assessment of the environmental impacts of the whole recycling process, it can be concluded from the above results that this recycling process is a green alternative with the following advantages. Firstly, BMW is innovatively applied as a green and renewable chemical for the reduction and conversion of different valuable metals in spent LIBs into the targeted products through the controlled reaction temperatures, and the reaction temperature can be reduced compared with those of traditional carbothermal and thermite based processes, resulting in a reduced input of energy. Secondly, the input of chemicals can also be greatly reduced due to the controlled conversion of different valuable metals into their recyclable states; the reduced consumption of chemicals also indicates that this recycling process can also prevent the contamination from the excessive unreacted chemicals, which can also make the subsequent separation process easier. Finally, this recycling process is a new concept that is mutually beneficial

for valuable metal recycling and high value-added gas production in a single process, and the treatment of waste gas can be easily achieved through the closed effluent gas treatment system. Therefore, this study is a green process with minimized inputs of energy and chemicals, and maximized outputs of different valuable products.

4. Conclusions

In this study, a novel biomass-waste-based thermochemical process with a significantly reduced roasting temperature was proposed towards efficient conversion and recycling of different metals from NCM as different products. It can be concluded that there are two main types of roasting reactions, namely a gas–solid reduction reaction by pyrolysis gases (*i.e.* H_2, CO, CO_2 and CH_4) at low roasting temperature and a solid–solid reaction (carbothermal reduction) by biochar at high roasting temperature. Correspondingly, the roasting products Li_2CO_3 and MeO (Me = Ni, Co or Mn) can be formed by a gas–solid reduction reaction at low roasting temperatures, while metallic Co, Ni and MnO are the dominant products for transition metals by carbothermal reduction at high roasting temperature. From the experimental results, nearly 100% of Co(III) and Mn(IV) in NCM are reduced to CoO and MnO along with the formation of Li_2CO_3 at the roasting temperature of 450 °C, and the oxides MeO can be further reduced into metallic Co and Ni, without any change of MnO during the further elevation of roasting temperature to 700 °C. Then, different valuable metals can be recycled based on different processing environments. Li was extracted by water-leaching and then Li_2CO_3 with a purity of 99.99% was recycled under the optimized leaching conditions of a roasting temperature of 550 °C, a retention time of 15 min and a pulp density of 20 g L^{-1}. Nearly all transition metals (98% Co, 99% Ni and 97% Mn) were leached under the optimized leaching conditions of a roasting temperature of 450 °C, a retention time of 15 min, and a H_2SO_4 concentration of 0.55 M for the roasting products at low roasting temperature, while 97% Co and 96% Ni were recovered in their metallic forms, with 98% MnO recovered as $MnSO_4$ after mild acid leaching for the roasting products at high roasting temperature. The ternary precursors $Ni_xCo_yMn_{1-x-y}(OH)_2$ can be recycled from the transition metal enriched leaching solution by co-precipitation after adjusting their molar ratios. Finally, the economic assessment of the whole recycling process suggests that it is a profitable route, with minimized inputs of energy and chemicals and maximized outputs of different valuable products.

Author contributions

Xiangping Chen: methodology, conceptualization, supervision, funding administration, and writing, review & editing; Yi Wang: investigation, methodology, data curation, and writing–original draft; Shuxuan Yan: data curation and writing–original draft; Lu Yuan: investigation, methodology, and data curation; Shubin Wang: methodology, funding administration, and writing – review & editing; Hongbo Liu: investigation and visualization; Junhu Xu: methodology, supervision, funding administration, and writing – review & editing.

Conflicts of interest

The authors declare no conflict of interest.

References

1 R. Tao, P. Xing, H. Li, Y. Wu, S. Li and Z. Sun, *ACS Sustainable Chem. Eng.*, 2021, **9**, 6318–6328.
2 J. Ordonez, E. J. Gago and A. Girard, *Renewable Sustainable Energy Rev.*, 2016, **60**, 195–205.
3 X. Zeng, J. Li and N. Singh, *Crit. Rev. Environ. Sci. Technol.*, 2014, **44**, 1129–1165.
4 W. Wang, Y. Zhang, L. Zhang and S. Xu, *J. Cleaner Prod.*, 2020, **249**, 119340.
5 Y. Zhang, W. Wang, Q. Fang and S. Xu, *Waste Manage.*, 2020, **102**, 847–855.
6 Y. Chen, P. Shi, D. Chang, Y. Jie, S. Yang, G. Wu, H. Chen, J. Zhu, F. Hu, B. P. Wilson and M. Lundstrom, *Sep. Purif. Technol.*, 2021, **258**, 118078.
7 W. Lv, Z. Wang, H. Cao, Y. Sun, Y. Zhang and Z. Sun, *ACS Sustainable Chem. Eng.*, 2018, **6**, 1504–1521.
8 Y. Fu, Y. He, Y. Yang, L. Qu, J. Li and R. Zhou, *J. Alloys Compd.*, 2020, **832**, 154920.
9 J. Xiao, B. Niu, Q. Song, L. Zhan and Z. Xu, *J. Hazard. Mater.*, 2021, **404**, 123947.
10 Q. Cheng, W. M. Chirdon, M. Lin, K. Mishra and X. Zhou, *Hydrometallurgy*, 2019, **185**, 1–11.
11 L. Li, L. Zhai, X. Zhang, J. Lu, R. Chen, F. Wu and K. Amine, *J. Power Sources*, 2014, **262**, 380–385.
12 E. Yuliusman, A. Silvia, F. Juwono, A. Yatim and E. Setiawan, *E3S Web of Conferences*, 2018, **67**, 03008.
13 X. Chen, J. Li, D. Kang, T. Zhou and H. Ma, *Green Chem.*, 2019, **21**, 6342–6352.
14 F. Meng, Q. Liu, R. Kim, J. Wang, G. Liu and A. Ghahreman, *Hydrometallurgy*, 2020, **191**, 105160.

15 X. Zeng, J. Li and B. Shen, *J. Hazard. Mater.*, 2015, **295**, 112–118.

16 X. Chen, D. Kang, J. Li, T. Zhou and H. Ma, *J. Hazard. Mater.*, 2020, **389**, 121887.

17 L. P. He, S. Y. Sun, X. F. Song and J. G. Yu, *Waste Manage.*, 2017, **64**, 171–181.

18 F. Pagnanelli, E. Moscardini, G. Granata, S. Cerbelli, L. Agosta, A. Fieramosca and L. Toro, *J. Ind. Eng. Chem.*, 2014, **20**, 3201–3207.

19 Y. Song and Z. Zhao, *Sep. Purif. Technol.*, 2018, **206**, 335–342.

20 Y. Yue, S. Wei, B. Yongjie, Z. Chenyang, S. Shaole and H. Yuehua, *ACS Sustainable Chem. Eng.*, 2018, **6**, 10445–10453.

21 Z. Cao, X. Zheng, H. Cao, H. Zhao, Z. Sun, Z. Guo, K. Wang and B. Zhou, *Chem. Eng. J.*, 2018, **337**, 256–264.

22 A. A. Nayl, M. M. Hamed and S. E. Rizk, *J. Taiwan Inst. Chem. Eng.*, 2015, **55**, 119–125.

23 S.-H. Joo, D. J. Shin, C. Oh, J.-P. Wang, G. Senanayake and S. M. Shin, *Hydrometallurgy*, 2016, **159**, 65–74.

24 W. F. Gao, X. H. Zhang, X. H. Zheng, X. Lin, H. B. Cao, Y. Zhi and Z. Sun, *Environ. Sci. Technol.*, 2017, **51**, 1662–1669.

25 B. K. Biswal, U. U. Jadhav, M. Madhaiyan, L. Ji, E.-H. Yang and B. Cao, *ACS Sustainable Chem. Eng.*, 2018, **6**, 12343–12352.

26 Z. Yu, H. Han, P. Feng, S. Zhao, T. Zhou, A. Kakade, S. Kulshrestha, S. Majeed and X. Li, *Bioresour. Technol.*, 2020, **297**, 122416.

27 Z. Sun, H. Cao, Y. Xiao, J. Sietsma, W. Jin, H. Agterhuis and Y. Yang, *ACS Sustainable Chem. Eng.*, 2016, **5**, 21–40.

28 H. Dang, N. Li, Z. Chang, B. Wang, Y. Zhan, X. Wu, W. Liu, S. Ali, H. Li, J. Guo, W. Li, H. Zhou and C. Sun, *Sep. Purif. Technol.*, 2020, **233**, 116025.

29 W. Wang, Y. Zhang, X. Liu and S. Xu, *ACS Sustainable Chem. Eng.*, 2019, **7**, 12222–12230.

30 J. Li, G. Wang and Z. Xu, *J. Hazard. Mater.*, 2016, **302**, 97–104.

31 Y. Tang, H. Xie, B. Zhang, X. Chen, Z. Zhao, J. Qu, P. Xing and H. Yin, *Waste Manage.*, 2019, **97**, 140–148.

32 D. Wang, X. Zhang, H. Chen and J. Sun, *Miner. Eng.*, 2018, **126**, 28–35.

33 D. H. Wang, H. Wen, H. J. Chen, Y. J. Yang and H. Y. Liang, *Chem. Res. Chin. Univ.*, 2016, **32**, 674–677.

34 Z. Zuo, Q. Yu, M. Wei, H. Xie, W. Duan, K. Wang and Q. Qin, *J. Therm. Anal. Calorim.*, 2016, **126**, 481–491.

35 Z. Cheng, G. Zhu and Y. Zhao, *Hydrometallurgy*, 2009, **96**, 176–179.

36 X. Zhang, D. Wang, H. Chen, L. Yang, Y. Yu and L. Xu, *Solid State Ionics*, 2019, **339**, 114983.

37 Y. Fu, Y. He, J. Li, L. Qu, Y. Yang, X. Guo and W. Xie, *J. Alloys Compd.*, 2020, **847**, 156489.

38 X. Zhang, H. Cao, Y. Xie, P. Ning, H. An, H. You and F. Nawaz, *Sep. Purif. Technol.*, 2015, **150**, 186–195.

39 Z. Wu, B. Zhang, S. Wu, G. Li, S. Zhao, Y. Li and B. Yang, *Fuel Process. Technol.*, 2019, **193**, 361–371.

40 K. Li, G. Chen, X. Li, J. Peng, R. Ruan, M. Omran and J. Chen, *Bioresour. Technol.*, 2019, **294**, 122217.

41 L. Chen, P. Wang, Y. Shen and M. Guo, *Bioresour. Technol.*, 2021, **323**, 124584.

42 V. S. Sikarwar, M. Zhao, P. Clough, J. Yao, X. Zhong, M. Z. Memon, N. Shah, E. J. Anthony and P. S. Fennell, *Energy Environ. Sci.*, 2016, **9**, 2939–2977.

43 X. Chen, Y. Wang, S. Li, Y. Jiang, Y. Cao and X. Ma, *Chem. Eng. J.*, 2022, **434**, 134542.

44 Y. Zhao, B. Liu, L. Zhang and S. Guo, *J. Hazard. Mater.*, 2020, **396**, 122740.

45 L. Xue, Y. Li, Q. Han, Q. Su, Y. Chen, J. Li, T. Lei, Y. Chen and J. Chen, *Ionics*, 2018, **24**, 2957–2963.

46 J. Mao, J. Li and Z. Xu, *J. Cleaner Prod.*, 2018, **205**, 923–929.

47 H. Zhang, G. Zhu, H. Yan, T. Li and Y. Zhao, *Metall. Mater. Trans. B*, 2013, **44**, 889–896.

48 F. Guo, X. Jia, S. Liang, N. Zhou, P. Chen and R. Ruan, *Bioresour. Technol.*, 2020, **298**, 122263.

49 M. Wang, Q. Tan and J. Li, *Environ. Sci. Technol.*, 2018, **52**, 13136–13143.

50 M. C. Biesinger, B. P. Payne, A. P. Grosvenor, L. W. M. Lau, A. R. Gerson and R. S. C. Smart, *Appl. Surf. Sci.*, 2011, **257**, 2717–2730.

51 Q. Jing, J. Zhang, Y. Liu, C. Yang, B. Ma, Y. Chen and C. Wang, *J. Phys. Chem. C*, 2019, **123**, 14207–14215.

52 L. Deng, Z. Xu, M. Wang, H. Shentu, X. Liu, J. Xiong, Y. Cheng, C. Wang, M. Zhou, J. Gao and Y. Xia, *Green Chem.*, 2021, **24**, 779–789.

53 Z. Huang, J. Zhu, R. Qiu, J. Ruan and R. Qiu, *J. Cleaner Prod.*, 2019, **229**, 1148–1157.

54 P. Li, S.-H. Luo, F. Su, L. Zhang, S. Yan, X. Lei, W. Mu, Q. Wang, Y. Zhang, X. Liu and P. Hou, *ACS Appl. Mater. Interfaces*, 2022, **14**, 11359–11374.

55 N. Gao, K. Chen, X. Lai and C. Quan, *Fuel*, 2021, **306**, 121676.

56 S.-L. Wu, J.-H. Kuo and M.-Y. Wey, *Int. J. Hydrogen Energy*, 2019, **44**, 13480–13489.

57 Y. Chai, M. Wang, N. Gao, Y. Duan and J. Li, *Chem. Eng. J.*, 2020, **396**, 125260.

58 Y. Chai, N. Gao, M. Wang and C. Wu, *Chem. Eng. J.*, 2020, **382**, 122947.

59 J. Mazumder and H. I. de Lasa, *Chem. Eng. J.*, 2016, **293**, 232–242.